Biomedical Physics &
Engineering Express

Endorsed by IPEM Institute of Physics and Engineering in Medicine
PURPOSE-LED PUBLISHING™

Numerical model of the irradiance field surrounding a UV disinfection robot

Biomedical Physics & Engineering Express

PAPER

Numerical model of the irradiance field surrounding a UV disinfection robot

Ludovic De Matteis[1,2], **Michael F Cullinan**[1,3] **and Conor McGinn**[1,3,*]

[1] Department of Mechanical, Manufacturing and Biomedical Engineering, Trinity College Dublin
[2] Université Paris-Saclay, Paris, France
[3] Akara Robotics, Dublin, Ireland
[*] Author to whom any correspondence should be addressed.

E-mail: mcginnc@tcd.ie

Keywords: medical robotics, UV radiation modelling, UV disinfection robot, ultraviolet germicidal irradiation

OPEN ACCESS

RECEIVED
16 November 2021

REVISED
2 May 2022

ACCEPTED FOR PUBLICATION
5 July 2022

PUBLISHED
10 August 2022

Abstract

Objective. New technologies, including robots comprising germ-killing UV lamps, are increasingly being used to decontaminate hospitals and prevent the spread of COVID-19 and other superbugs. Existing approaches for modelling the irradiance field surrounding mobile UV disinfection robots are limited by their inability to capture the physics of their bespoke geometrical configurations and do not account for reflections. The goal of this research was to extend current models to address these limitations and to subsequently verify these models using empirically collected data. *Approach.* Two distinct parametric models were developed to describe a multi-lamp robotic UV system and adapted to incorporate the effects of irradiance amplification from the device's reflectors. The first model was derived from electromagnetic wave theory while the second was derived from conservation of energy and diffusion methods. Both models were tuned using data from empirical testing of an existing UV robot, and then validated using an independent set of measurements from the same device. *Results.* For each parameter, predictions made using the conservation of energy method were found to closely approximate the empirical data, offering more accurate estimates of the 3D irradiance field than the electromagnetic wave theory model. *Significance.* The versatility of the proposed method ensures that it can be easily adapted to different embodiments, providing a systematic way for researchers to develop accurate numerical models of custom UV robots, which may be used to inform deployment and/or to improve the accuracy of virtual simulation.

1. Introduction

Growing concerns caused by the spread of multi-drug resistant organisms (MDROs) and SARS-CoV-2 have motivated the development of new disinfection technologies for use in hospitals and other healthcare settings. Among the most compelling emerging technologies is ultraviolet germicidal irradiation (UVGI), a non-touch method of disinfection that achieves microbe inactivation through the transmission of light with wavelengths in the range of 200–280 nm, commonly referred to as the UVC spectrum. UVGI sources include technologies that generate pulsed UV light that emits radiation across a broad range of wavelengths (200–320 nm) or continuous narrow band radiation, normally close to 260 nm which is considered the optimal wavelength for microbial inactivation [1, 2]. The former category of devices have normally used pulsed xenon (PX-UV) technology (i.e. [3–5]) while the latter have used low-pressure mercury lamps (LPML) (i.e. [6, 7]) or LEDs (i.e. [8]). An emerging UVGI technology, known as far-UV, emits continuous narrow band irradiation at 222 nm using KrCl excimer lamps. UVGI has advantages over manual disinfection using biocides, including effectiveness against broad-spectrum organisms, lack of harmful residuals, reduced labour and consumable costs, and relative simplicity of operation within a healthcare environment.

The critical UVC dose needed to inactivate most common pathogens has been established, and it typically ranges from 1.5–9 mJ cm^{-2} for a log-1 reduction (also known as the D90 value) [9]. However, in the absence of UVC sensitive test cards or environmental sensing devices, it can be difficult to estimate the UVC dose absorbed by surfaces in the vicinity of UVGI

devices since large gradients exist in the irradiance field, which vary nonlinearly as function of distance from the UVC source and can be further affected by other aspects of the device's embodiment.

Many techniques exist in the literature to describe models of light propagation. The light fluence rate has been shown to be proportional to the distance from the source, and have been modelled in many applications using the inverse square law [10–13]. However, while it is sufficiently accurate for general lightning purposes [14], when applied to UVGI it loses accuracy in the near-field where most of the germicidal effects occur [15, 16].

Other models of light fluence rate have been proposed. Jacques developed a model that used light point sources, diffusion theory and conservation of energy to describe light propagation in biological tissues [17]. Diffusion theory has been used in several light modelling applications along with Monte Carlo simulations [18, 19]. Diffusion theory loses accuracy near sources where the rate of change of irradiance is sufficiently large that it cannot be approximated as linear within a region of a few diffusion lengths in size. The error that occurs near the source creates residual errors far from the source. Therefore, these models give a good prediction of the shape of the light fluence but have issues accurately predicting its absolute value [17]. Diffuse models of point sources have also been extended to model line sources and planar sources as collection of diffuse points sources [17].

View factor models use methods from thermal irradiation and have been found to effectively predict lamp irradiance at any distance. However, view factors can only accurately depict interactions with diffuse surfaces but lose accuracy when reflective surfaces are to be modelled [16]. These models have been applied to light fluence rate in the near field (less than one meter) with modelling of diffusive or specular models for the reflective surfaces [20, 21]. However, while view factors provide accurate prediction of the lamp fluence rate in the near field, they require more effort to accurately model reflective surfaces.

Ray tracing is a widely used approach to describe light interaction with its environment and has been adapted to model UVGI processes [22–24]. A recent paper by Mishra *et al* used ray tracing simulations to model reflections within a UVC disinfection chamber to ensure uniform radiation distribution [25].

While mathematical models exist for describing the irradiance surrounding a UVC source, the optimum way to model more complex systems comprising multiple UVC lamps and reflective surfaces remains undetermined. Kowalski has developed models to specifically describe the behaviour of UVGI systems, especially in the near field region (less than one meter) [20, 21]. He worked on modelling the fluence rate at a point inside a reflective enclosure using a view factor approach, modelling the reflective surfaces as purely specularly reflective. However, the author concludes stating that fluence rate at a point cannot be accurately measured by a sensor and thus no conclusion on the model's exact accuracy can be drawn.

Although view factors appears to be more accurate for predicting fluence rate, configuring it for different UVGI systems is a complex and computationally expensive task. Conversely, the other models are simpler to setup but fail in their ability to accurately model reflections. The primary objective of this research was to extend current models to more accurately represent the irradiance field surrounding a UVC robot, and to subsequently verify these models using empirically collected data. In the next section, we present the development of the mathematical models used with the UVC apparatus and outline the details of the sensitivity analysis. We compare the performance of both models in section 3, along with results from our sensitivity analysis. This is followed by a discussion of our findings and summary of our conclusions in sections 4 and 5 respectively.

2. Methods

The methods developed in this work have been adapted to model an existing robotic UVGI platform developed by Akara Robotics (https://www.akara.ai/). This robot met the inclusion criteria of being a mobile UVC disinfection robot with a heterogeneous irradiation field (emergent from the interaction of multiple UVC lamps and a reflector) that could not be accurately modelled by point or line sources alone. The company developing this robot also provided access that enabled us to collect empirical measurements which were necessary to refine and validate the models. The Akara robot system was composed of three vertical low pressure UVC lamps[4] surrounded by three reflective surfaces, as shown in figure 1. This configuration and use of reflective surfaces is intended to amplify the light in front of the robot, while blocking light from escaping behind, making it safe for people to operate in the robot's rear vicinity. The UVGI platform being used in a clinical deployment is shown in figure 2.

To model the robot platform, we consider each lamp to be a line source, which can be modelled as a collection of point sources, as outlined in [17]. Two point source models were evaluated: the wave propagation model and energy diffusion model.

2.1. Wave propagation model

The first point source model was based on electromagnetic wave theory. We assumed that the environment was isotropic (i.e. the light propagates uniformly in all directions). The irradiance (or energetic irradiance), I_R, was defined as:

[4] Specs of the lamps can be found at: https://www.assets.signify.com/is/content/PhilipsLighting/fp928048604003-pss-en_au.

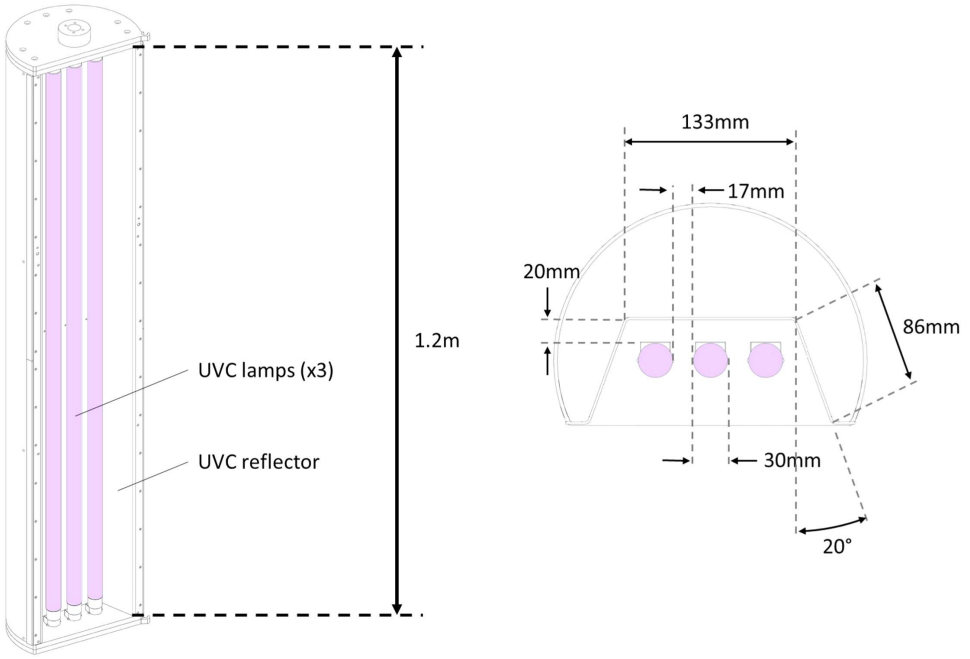

Figure 1. Schematic of the UVC lamp arrangement modelled in this paper. The system comprises three LPML UVC lamps (shown in blue) surrounded by a bespoke metallic reflector and mounted within a cylindical column.

Figure 2. A photograph of the UVC disinfection robot modelled in this paper being used in a hospital.

$$I_R = \frac{\partial \Phi_e}{\partial A} \tag{1}$$

where Φ_e is the radiant flux on a surface and dA the infinitesimal area of the surface.

The radiant flux, Φ_e, of a surface Σ is the flux of the Poynting vector $\vec{S}$ through this surface.

$$\Phi_e = \oint_{\Sigma} \vec{S}.\vec{dA} \tag{2}$$

To compute the Poynting vector, one can obtain the general solution of Maxwell's law of propagation, known as d'Alembert's equation:

$$E = E_0 \exp(\pm i(k_x x + k_y y + k_z z - \omega t)) \tag{3}$$

where k_x, k_y and k_z are the 3D wave vector components, ω the frequency of the magnetic field, and E_0 an unknown constant depending on the source characteristics.

For point source modelling, we can assume spherical distribution [17] that leads, using Curie's Symmetry Principle, to:

$$\vec{E}(\vec{r},\, t) = \frac{E_0}{r} e^{\pm i(kr-\omega t)} \vec{e_r} \tag{4}$$

where r the distance from the source to the surface in the direction of propagation $\vec{e_r}$ and k the norm of the wave vector i.e. $k = \|(k_x \quad k_y \quad k_z)\|$.

Thus, we can compute Poynting's vector:

$$\begin{aligned} \|\vec{S}\| &= \epsilon_0 c \, \|\vec{E}\|^2 \\ \|\vec{S}\| &= \frac{\epsilon_0 c E_0^2}{r^2} \end{aligned} \tag{5}$$

where ϵ_0 is the vacuum permittivity and c the light celerity, which are both known parameters. Using equations (2) and (1) we obtain:

$$I_R(r) = \frac{\epsilon_0 c E_0^2}{r^2} \vec{e_r}.\vec{dA} \qquad [W/m^2] \tag{6}$$

This model incorporates the inverse square law which naturally describes the fluence at a point. To describe the irradiance at a surface, Lambert's cosine law was added.

Using the inverse square law model of a point source to predict fluence surrounding a UVGI platform introduces approximation errors for points close to the source [9, 12, 21]. This arises because the model does not consider the finite size of the object of interest and assumes a perfect point source. This model also makes the assumptions of an isotropic environment and that the medium of propagation is a vacuum.

2.2. Energy diffusion model

In [17], Jacques presented a different model for light fluence rate based on the diffusion and conservation of energy. Here we propose an extension of this model to describe irradiance field using Lambert's cosine law.

The point source is modelled as a sphere emitting the energy S_0. Invoking the conservation of energy, the integral of the permeability of air (μ_a) multiplied by the energetic irradiance over all space is equal to the source energy S_0. Considering a constant permeability of air and a isotropic environment, it translates to an integral over the distance:

$$\int_0^\infty \mu_a I_R(r) 4\pi r^2 dr = S_0 \tag{7}$$

In spherical coordinates, the solution $I_R(r)$ of the diffusion equation should include the term $exp(-r/\delta)$ [17]. Therefore, the general solution is:

$$I_R(r) = \frac{S_0 exp(-r/\delta)}{4\pi\mu_a \delta^2 r} \vec{e_r}.\vec{dA} \qquad [W/m^2] \tag{8}$$

Where δ is an unknown parameter corresponding to the attenuation length of light, depending on the wavelength and the environment.

This model makes similar assumptions as the wave propagation model regarding the use of point source as well as an isotropic and homogeneous environment. Moreover, diffusion theory appears to lose accuracy in parts where the gradients of irradiance are changing faster than can be considered linear within a region of a few diffusion lengths. This happens especially in the near field (less than one meter) and can yield consequent errors. These errors propagate through the integration and create residual errors with distance from the source. However, these errors decrease as we get further from the lamp as the surface of integration becomes larger. Diffusion models are therefore by construction more accurate further from the source [17].

2.3. Modelling reflective surfaces and custom UVC lamp housings

To account for the reflective surfaces of the robot, virtual lamps corresponding to the reflections of the three lamps on each of the reflectors are added. These lamps emit a reduced irradiance depending on the material of the reflectors. For our use-case, we consider a reflection coefficient of 20% (i.e 20% percent of the power of the parent lamp) [26]. To replicate the geometry of the light column on the Akara robot platform,the irradiance from each lamp, real and virtual, was constrained to lie within the boundaries defined by the reflector. A point is then considered in the field of irradiation of the lamp if its angle with respect to the lamp position is within the sector of the field of irradiation. This geometry is illustrated in figure 3. This method allows us to model different complex structures of line/point sources and reflectors. Since most surfaces are very poor reflectors of light in the UVC range and given the rapid reduction in UVC fluence with distance, it is assumed that modelling the reflections from other surfaces in the environment will provide negligible improvements in model performance.

2.4. Experimental protocol

First, an empirical model of the irradiance field surrounding the UVC robot was created from real-world sensor measurements. The UVC robot was positioned in the middle of a large room, away from surfaces that might reflect UVC light. Using a tape measure and a protractor, a grid spanning a radial distance of 3 m and an arc of 120° was traced on the floor. Discrete measurements of the UVC field surrounding the robot were taken in radial intervals of 0.5 m and 30°, as illustrated in figure 4. At each spatial location, measurements were taken at four different heights: 0 m (i.e. ground level), 0.5 m, 1 m and 1.5 m, measured using a measuring rod. For each measurement, the sensor was orientated directly towards the centre of the grid. Due to the symmetry of the UVC lamp and reflector assembly, measurements were taken on one side only. UVC readings were taken using an Omega HHUV254SD UV meter[5], a device capable of measuring UV intensity in the range of 240 nm to

[5] Specs of the UV meter can be found at: https://assets.omega.com/manuals/test-and-measurement-equipment/light-meters/M5083.pdf.

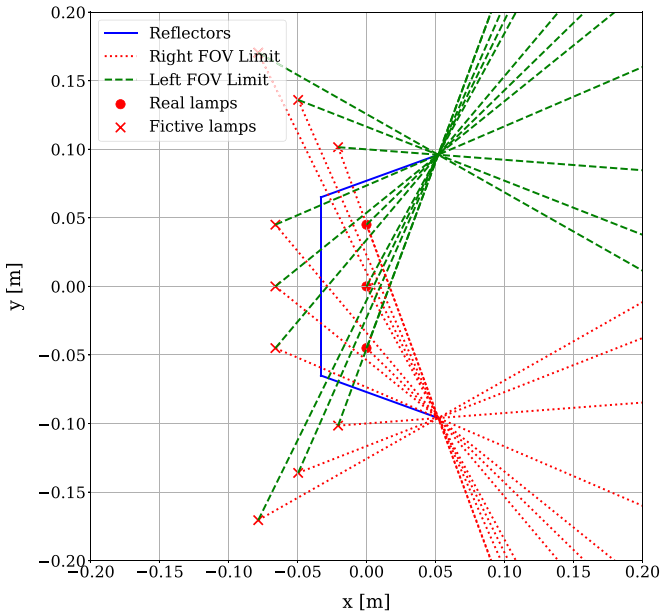

Figure 3. Plan projection showing the virtual lamps (red crosses) superimposed on the geometry of the lamp arrangement (shown in red dots) and reflective barrier (blue line). The field of irriadiation of both the real and virtual lamps is indicated by dotted lines.

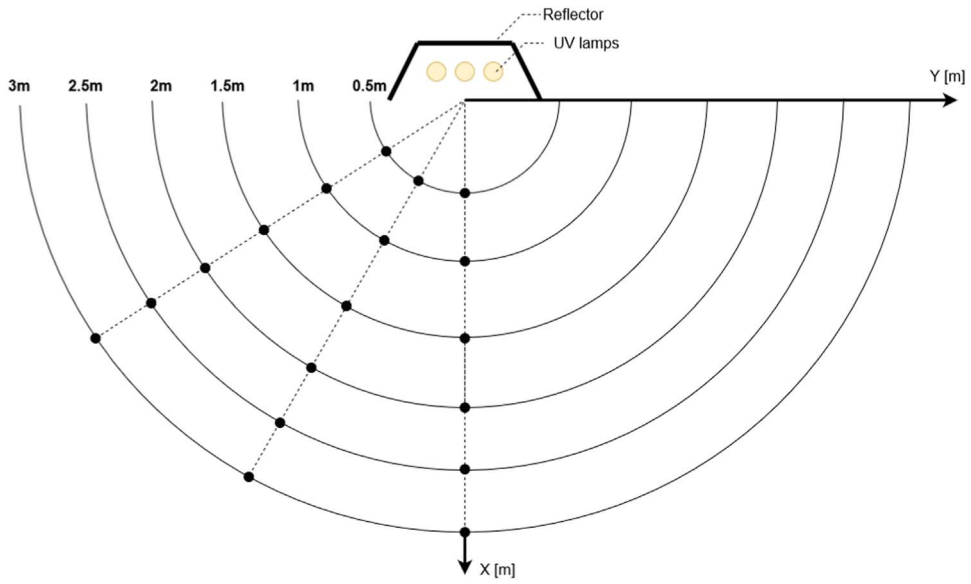

Figure 4. UVC measurements were taken at 6 radial distances (0.5 m, 1 m, 1.5 m, 2 m, 2.5 m, 3 m) and three orientations (0°, 30°, 60°), as indicated by the black dots in the figure. At each of these points, measurements were taken at 4 different heights (0 m, 0.5 m, 1 m, 1.5 m). This figure is not drawn to scale.

390 nm with an accuracy of ±4% of the full scale reading. We estimated the angle measurements were accurate to approximately ±0.3°, leading to a maximum positional error, accounting for propagation over distance, of approximately ±1.57 cm. Radial distance and height measurements were accurate to approximately ±0.1–0.2 cm. Using this approach, the emperically determined UV irrradiance field is plotted in figure 5.

3. Results

The empirical measurements of the UVC field surrounding the UVGI device are tabulated in table 1.

For both models, we conducted an optimization process to find the unknown parameters (constants) of the models given the empirical measurements in table 1. With these parameters defined, we subsequently compared the performance of both models.

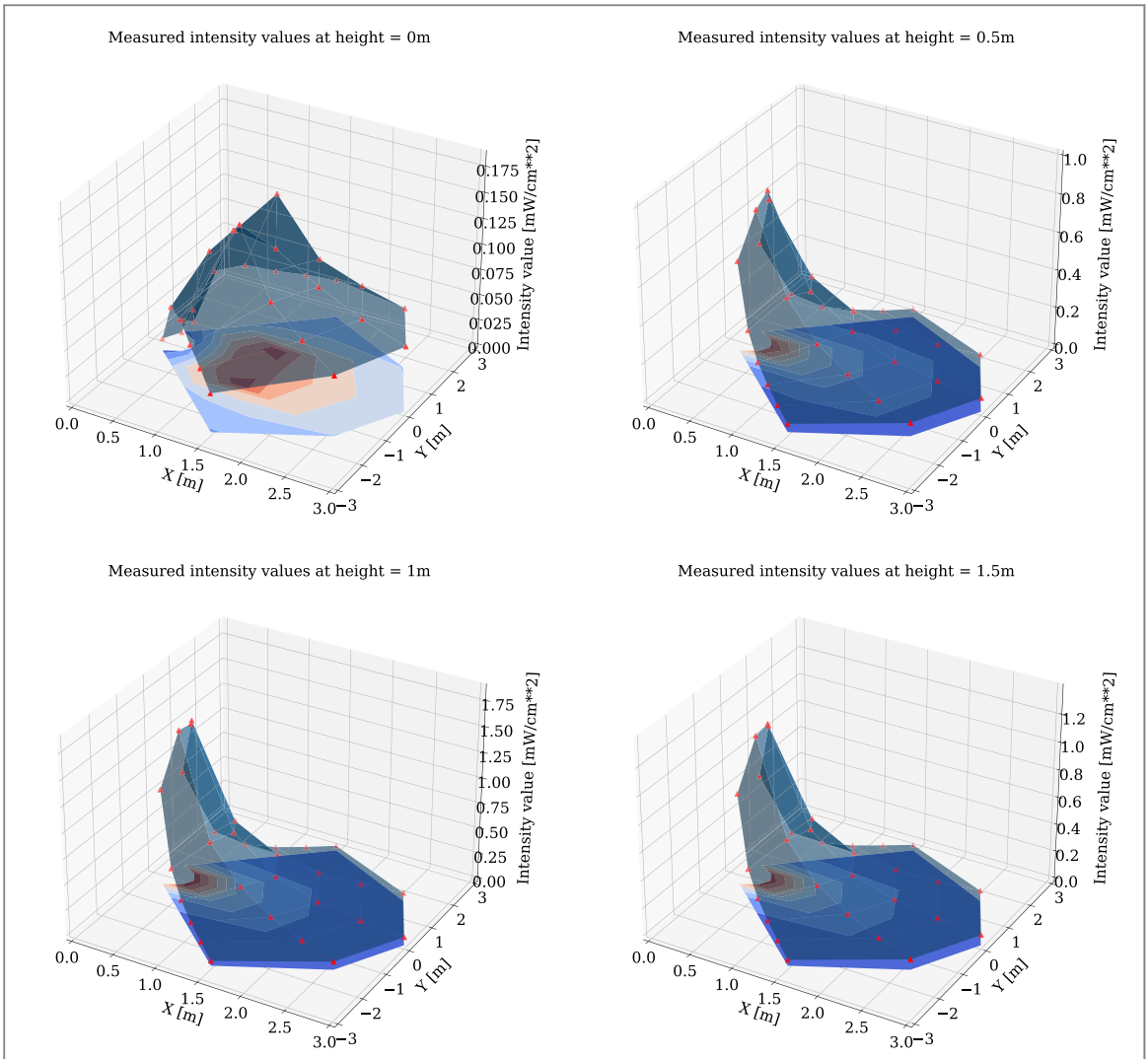

Figure 5. Graphic visualization of the measurements of the UVC irradiance field. The graphs use the same x/y coordinate system as in figure 4, with the UVC lamp column centered at the origin. The z axis corresponds with the UVC intensity measurement reading, measured in mW cm^{-2}. Graphs were generated using Python.

Table 1. Measurements of the UVC irradiance field. All measurements are in mW cm^2.

Height 0m	*0.5m*	*1m*	*1.5m*	*2m*	*2.5m*	*3m*
0 deg	0.038	0.128	0.122	0.097	0.078	0.064
30 deg	0.019	0.115	0.155	0.097	0.076	0.059
60 deg	0.012	0.059	0.062	0.053	0.046	0.038
Height 0.5m	*0.5m*	*1m*	*1.5m*	*2m*	*2.5m*	*3m*
0 deg	0.836	0.370	0.223	0.129	0.095	0.073
30 deg	0.754	0.376	0.216	0.144	0.095	0.070
60 deg	0.480	0.194	0.107	0.074	0.052	0.044
Height 1m	*0.5m*	*1m*	*1.5m*	*2m*	*2.5m*	*3m*
0 deg	1.556	0.612	0.298	0.171	0.114	0.081
30 deg	1.527	0.592	0.310	0.178	0.116	0.080
60 deg	0.947	0.316	0.157	0.096	0.067	0.048
Height 1.5m	*0.5m*	*1m*	*1.5m*	*2m*	*2.5m*	*3m*
0 deg	1.155	0.477	0.233	0.145	0.106	0.076
30 deg	1.094	0.457	0.241	0.154	0.105	0.076
60 deg	0.671	0.229	0.129	0.084	0.062	0.043

3.1. Wave propagation model

The model based on electromagnetic wave theory and presented section 2.1 presents a unique unknown variable denoted as E_0 in equation (6). For the optimization process, this equation is written as:

$$I_R(r,\, h,\, \theta) = \frac{E}{r^2}\vec{e_r}.\vec{dA} \qquad [W/m^2] \tag{9}$$

Where E is the only unknown and the input parameters r, h, θ are known for each of the measurements taken.

We use a weighted squared error cost function to minimise the number of points far from the measured values. The weighting is designed to have a more precise model for our desired use case, i.e. in front of the lamps at 1 m distance and heights from 1 m to 1.5 m. As the output value of the model is scalar, we can use the following form of the weighted squared error criterion:

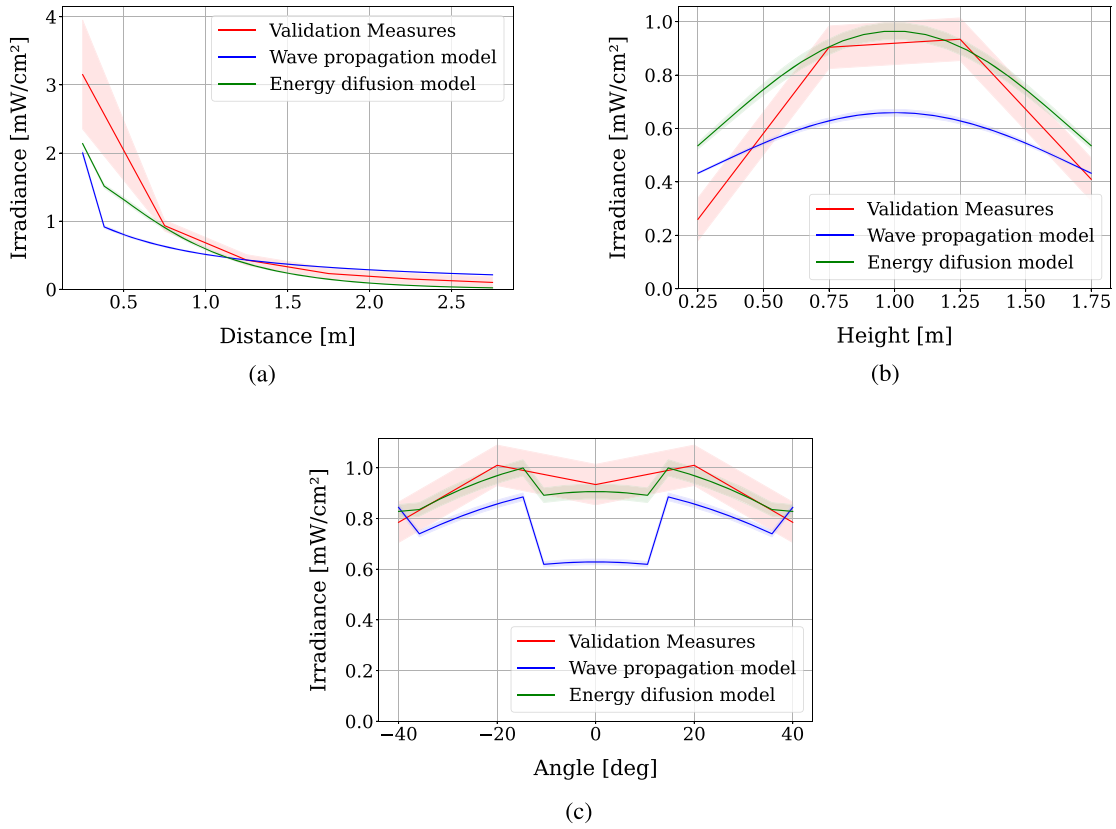

Figure 6. Visual comparison of the two models prediction with experimental measurements. The measurements taken and their uncertainty is plot in red. The wave propagation model and the energy diffusion model are respectively in blue and green. The models also presents an uncertainty range computed by considering the ±2 cm uncertainty on the distance measurements. (a) Comparison of the distance influence on the validation measurements and the models predictions around *height* = 1.25 m and *angle* = 0 deg. (b) Comparison of the height influence on the validation measurements and the models predictions around *distance* = 0.75m and *angle* = 0 deg. (c) Comparison of the angle influence on the validation measures and the models predictions around *height* = 1.25m and *distance* = 0.75 m.

$$L(x) = \sum_{d\in\mathcal{D}}\sum_{h\in\mathcal{H}}\sum_{a\in\mathcal{A}} \times (\hat{y}(x, d, h, a) - y(d, h, a))^2 W(d, h, a)$$

where $\mathcal{D}$ is the set of distances where the measurements where taken, $\mathcal{H}$ the set of heights and $\mathcal{A}$ the set of angles, $\hat{y}$ is the output value of model we use, y the ground truth and x the unknown parameters (for the wave propagation model, x is the only unknown parameter, E). The weighting W depends on the distance, height and angle considered.

The unknown values are initialized at 1 and fed to an optimization process using the Nelder-Mead method. The result led to $E = 1.51$W.

3.2. Energy diffusion model

The diffusion model, discussed in section 2.2, presents two unknown parameters and is written for the optimization process as:

$$I_R(r) = \frac{Eexp(-kr)}{r}\vec{e_r}.\vec{dA} \quad [W/m^2] \qquad (10)$$

Where E and k are two unknown parameters.

An optimization process using the same loss function with same weights and initialization as used for model 1 was implemented, leading to parameter values of $E = 4.49$ W m^{-1} and $k = 1.98$ m^{-1}.

3.3. Model validation

To compare model performance, we built a second dataset of experimental measurements taken at different points using the same experimental protocol as before. Measurements were taken heights of 0.25 m, 0.75 m, 1.25 m and 1.75 m, and distances of 0.25 m, 0.75 m, 1.25 m, 1.75 m, 2.25 m and 2.75 m, and angles of 0°, 20° and 40°. A visual comparison showing the models' predictions alongside the empirical data is presented in figure 6. These graphs were generated using Python (version 3.6) with numpy and matplotlib.

The energy diffusion model was found to have better overall accuracy than the wave propagation model for our range of parameters. This seems to confirm the hypothesis that that the wave propagation model improves its accuracy at longer distances where effects of reflection or absorption in the medium start to decrease; this can be observed most notably in figure 6(a). Although the energy diffusion model boasts better short range performance, both models seem to lose accuracy closer to the lamp. The energy diffusion model better captures the influence of offset angle than the wave propagation model figure 6(c);

Table 2. Energy diffusion model first order and total order sensitivity indexes computed using Sobol's method for ANOVA.

Parameter	First order	Total order
Distance	0.492 ± 0.063	0.726 ± 0.086
Height	0.229 ± 0.065	0.467 ± 0.057
Angle	0.033 ± 0.024	0.068 ± 0.012

Table 3. Energy diffusion model Second order sensitivity index computed using Sobol's method for ANOVA.

Parameter #1	Parameter #2	Second order
Distance	Height	0.216 ± 0.118
Height	Angle	-0.003 ± 0.100
Angle	Distance	0.016 ± 0.069

this further demonstrates that this model better predicts the effects of close range reflections. However, figure 6(b) suggests that the energy diffusion model has issues with limit conditions, overestimating the value of the irradiance for low and high heights. This may indicate that the Lambert's cosine law isn't sufficient to entirely predict the effects of the surface orientation near limit conditions —i.e. when angles are too high.

3.4. Input sensitivity analysisdata

A sensitivity analysis was conducted to determine the sensitivity of the energy diffusion model to its inputs. This was performed using an analysis of variance (ANOVA), a method of sensitivity analysis that has been commonly used in other studies [27–30]. The python library SALib[6] was used to generate the parameters list and to compute the sensitivity indexes using Sobol's method, a technique that is capable of determining the first-order, second-order and total-order sensitivity indexes of the input parameters [27, 31].

A list of parameters was defined using the following range for the distance, height and angle inputs of the models:

$$\begin{aligned} distance &\in [0.5;\ 3] \\ height &\in [0;\ 1.5] \\ angle &\in [0;\ 60] \end{aligned} \tag{11}$$

Tables 2 and 3 present results for the energy diffusion model. The first order sensitivity index describes the proportion of the output uncertainty due to each of the parameters independently (i.e. not involving a combination of parameters). It emerged, based on the first order sensitively index of the respective parameters, that uncertainty on the planar distance from the lamps to the point explains half of the output uncertainty, while the height of the point accounts for a quarter. The uncertainty on the angle of the point, however, accounts for less than 5% of the output uncertainty.

Similar patterns appear when considering parameters' interactions. The second order sensitivity indexes indicates that height and distance interaction is the most important one, explaining about 21% of the total output uncertainty. The total order sensitivity index takes into account both the uncertainty due to the parameters independently and to parameter interactions.

[6] https://salib.readthedocs.io/en/latest/

4. Discussion

This study investigated the modelling of the irradiance field surrounding a UVC robot using two parametric models. These models expanded on simple point and line-source light models since they incorporated a bespoke configuration of UVC lamps as well as reflectors. Using empirical measurements taken from the robot's environment, we implemented an optimization process to determine the values of the parameters we could not obtain from direct measurements. For each model, we used a weighted mean squared error loss function to prioritize a good fit in the region around the nominal point of use of the robot. On comparison of both models, we found that the energy diffusion model based on the conservation of energy, presented the best overall results. The wave propagation model, based on electromagnetic wave theory, was found to have noticeably reduced accuracy at short distances from the lamp and when considering reflections close to the lamps. The effect of reflection on this model was especially noticeable when considering points in the field of view of all virtual lamps (i.e. in front of the robot). The model prediction errors of the virtual lamps irradiance added up leading to a consequent prediction error that reduced when the measurement point was outside the field of view of the virtual lamps.

We also conducted a sensitivity study on the energy diffusion model to determine the output uncertainty due to three distance parameters: radial distance, height above the ground, and orientation from the normal axis of the UVC robot. This study showed that approximately 50% of the total output uncertainty can be explained by the distance parameter alone, while this value increases to 73% when considering its interactions with the two other parameters. The height parameter further explains 23% of the output uncertainty and its interactions take this value to 47%. The uncertainty on the angle parameter has far less effect on the output. We conclude that the lowest possible uncertainty on the distance and height input parameters is required to predict the irradiance with good accuracy. Analysis of these outcomes allows us to give some important recommendations for using this model. First, when using the model, one should aim at having a distance input as precise as possible since uncertainty on this parameter will propagate significantly to the output. Second, the height of the point from the base of the lamp is quite important and will require a low uncertainty; uncertainty on the angle has less effect.

We observe several limitations of this study. Firstly, since the robot used in this analysis used low-pressure mercury lamps that irradiate continuously, the degree to which the models describe the irradiance field of UVGI devices that emit broadband pulsed UV light (such as PX-UV technologies) remains unclear. Second, we acknowledge some measurement errors were likely present. However, we deemed that their magnitude was small relative to the data and are unlikely to have affected the results. And thirdly, since it was not possible to get accurate UVC measurements within 0.5 m of the robot,[7] the accuracy of the model in the near-field of the UVC lamp remains unclear.

Additionally, this work presents only analytical models that can be easily implemented on embedded systems. However, these models have limited accuracy and more complex models such as view factors may yield better accuracy at the cost of greater computation. Better identification of the reflective surfaces may also help to improve the results of the models, since the parameters of these surfaces are used to model reflections through fictive sources, and any error would be propagated to these sources.

5. Conclusions

In this paper, we presented a methodology to construct and evaluate a model for the irradiance field around a bespoke UVGI platform. We extended the applicability of two models previously used in the literature and compared both. Through a sensitivity analysis, we also determined the most important parameters to reduce uncertainty in the models predictions.

Our results showed a clear difference between models, with one of them achieving greater accuracy in modelling the effect of reflections and in the prediction of the irradiance field. The improved performance was most noticeable at a medium range of around 1 m. Our sensitivity analysis showed that the radial distance and height above the ground (relative to the UVC source) are the two major factors influencing the intensity of the irradiance field surrounding the robot. Therefore, when using the model, one should aim at having a distance and height inputs as accurate as possible to avoid error propagation in the predicted irradiance values. The orientation of the robot had less influence on the irradiance prediction, provided that point of interest was within the field of irradiation.

The results of this work show promising prediction performance. This facilitates improved near-field prediction of irradiation levels surrounding mechanically distinct UVC robot embodiments. Future work will explore the applicability of using the model to simulate a UVGI procedure in a virtual hospital environment to optimize the placement of UVGI device in the room. This has the potential enable room disinfection procedures to be generated virtually using machine learning and other optimization techniques.

[7] At short distances, the sensor was unable to register UVC irradiance from the extremities if the UVC lamps due to the large incident angle.

Acknowledgments

Funding for the project was provided for a grant from Science Foundation Ireland, as part of their COVID-19 Rapid Response Initiative (grant ID: 20/COV/0021). We are also grateful to Akara Robotics for providing access to the robotic platform used in this study.

Conflict of Interest

Author 2 and Author 3 declare a conflict of interest due to their involvement as shareholders of X, a company involved in the development of UVGI technology.

ORCID iDs

Conor McGinn https://orcid.org/0000-0001-9019-6809

References

[1] Batista L F, Kaina B, Meneghini R and Menck C F 2009 How dna lesions are turned into powerful killing structures: insights from uv-induced apoptosis *Mutation Research/Reviews in Mutation Research* **681** 197–208

[2] Sholtes K and Linden K G 2019 Pulsed and continuous light uv led: microbial inactivation, electrical, and time efficiency *Water Res.* **165** 114965

[3] Hosein I, Madeloso R, Nagaratnam W, Villamaria F, Stock E and Jinadatha C 2016 Evaluation of a pulsed xenon ultraviolet light device for isolation room disinfection in a united kingdom hospital *American Journal of Infection Control* **44** e157–61

[4] Casini B, Tuvo B, Cristina M L, Spagnolo A M, Totaro M, Baggiani A and Privitera G P 2019 Evaluation of an ultraviolet c (uvc) light-emitting device for disinfection of high touch surfaces in hospital critical areas *International Journal of Environmental Research and Public Health* **16** 3572

[5] Nerandzic M M, Thota P, Sankar T, Jencson A, Cadnum J L, Ray A J, Salata R A, Watkins R R and Donskey C J 2015 Evaluation of a pulsed xenon ultraviolet disinfection system for reduction of healthcare-associated pathogens in hospital rooms *Infection Control & Hospital Epidemiology* **36** 192–7

[6] Umezawa K, Asai S, Inokuchi S and Miyachi H 2012 A comparative study of the bactericidal activity and daily disinfection housekeeping surfaces by a new portable pulsed uv radiation device *Current Microbiology* **64** 581–7

[7] Penno K, Jandarov R A and Sopirala M M 2017 Effect of automated ultraviolet c-emitting device on decontamination of hospital rooms with and without real-time observation of terminal room disinfection *American Journal of Infection Control* **45** 1208–13

[8] Messina G, Burgassi S, Messina D, Montagnani V and Cevenini G 2015 A new uv-led device for automatic disinfection of stethoscope membranes *American Journal of Infection Control* **43** e61–6

[9] Kowalski W 2010 *Ultraviolet Germicidal Irradiation Handbook: UVGI for Air and Surface Disinfection* (Germany: Springer Science & Business Media)

[10] Ryer A and Light V 1997 *Light Measurement Handbook*

[11] Voudoukis N and Oikonomidis S 2017 Inverse square law for light and radiation: A unifying educational approach *European Journal of Engineering and Technology Research* **2** 23–7

[12] Koval'skii V, Sapritskii V, Stolyarevskaya R and Khlevnoy B 1989 Correction to the inverse square law *Meas. Tech.* **32** 946–51
[13] Conroy J, Thierauf C, Rule P, Krause E, Akitaya H, Gonczi A, Korman M and Scheutz M 2021 Robot development and path planning for indoor ultraviolet light disinfection *2021 IEEE International Conference on Robotics and Automation (ICRA), IEEE (Xi'an, China, 30 May 2021–05 June)* (IEEE: Picastaway, NJ) pp 7795–801
[14] Schlosser W, Schmidt-Kaler T and Milone E F 1991 *Photography of the Sun and Stars* (New York, NY: Springer New York) pp 77–82
[15] Narayanan V A and Narayanan R 1999 Inverse-square law of light with airy's disk *The Physics Teacher* **37** 8–9
[16] Kowalski W J and Bahnfleth W P 2000 Effective uvgi system design through improved modeling *ASHRAE Transactions* **106** 721 Copyright—Copyright American Society of Heating, Refrigeration and Air Conditioning Engineers, Inc. 2000; Dernière mise à jour—2014-05-20; CODEN—ASHTAG.
[17] Jacques S L 1998 Light distributions from point, line and plane sources for photochemical reactions and fluorescence in turbid biological tissues *Photochem. Photobiol.* **67** 23–32
[18] Flock S, Patterson M, Wilson B and Wyman D 1989 Monte carlo modeling of light propagation in highly scattering tissues. i. model predictions and comparison with diffusion theory *IEEE Trans. Biomed. Eng.* **36** 1162–8
[19] Star W M 1995 Diffusion theory of light transport *Optical-Thermal Response of Laser-Irradiated Tissue* (Berlin: Springer) pp 131–206
[20] Kowalski W 2001 Design and Optimization of UVGI Air Disinfection Systems *PhD Thesis* Penn State, USA 01
[21] Kowalski W, Bahnfleth W and Mistrick A 2005 A specular model for uvgi air disinfection systems *IUVA News* **7** 19–26
[22] Govaerts Y and Verstraete M 1998 Raytran: a monte carlo ray-tracing model to compute light scattering in three-dimensional heterogeneous media *IEEE Trans. Geosci. Remote Sens.* **36** 493–505
[23] Leutz R and Annen H P 2007 Reverse ray-tracing model for the performance evaluation of stationary solar concentrators *Sol. Energy* **81** 761–7
[24] Hou M, Pantelic J and Aviv D 2021 Spatial analysis of the impact of uvgi technology in occupied rooms using ray-tracing simulation *Indoor Air* n/a (https://doi.org/10.1111/ina.12827)
[25] Mishra S, Singh D and Wanare H 2022 Chaotic cavity design of a uv-c disinfection chamber for uniform radiation distribution *Appl. Opt.* **61** 890–7
[26] Campos J, Fontecha J, Pons A, Corredera P and Corróns A 1998 Measurement of standard aluminium mirrors, reflectance versus light polarization *Meas. Sci. Technol.* **9** 256
[27] Saltelli A, Annoni P, Azzini I, Campolongo F, Ratto M and Tarantola S 2010 Variance based sensitivity analysis of model output. design and estimator for the total sensitivity index *Comput. Phys. Commun.* **181** 259–70
[28] Tang Y, Reed P, Wagener T and Werkhoven K v 2007 Comparing sensitivity analysis methods to advance lumped watershed model identification and evaluation *Hydrol. Earth Syst. Sci.* **11** 793–817
[29] Lenhart T, Eckhardt K, Fohrer N and Frede H-G 2002 Comparison of two different approaches of sensitivity analysis *Physics and Chemistry of the Earth, Parts A/B/C* **27** 645–54
[30] Saltelli A, Aleksankina K, Becker W, Fennell P, Ferretti F, Holst N, Li S and Wu Q 2019 Why so many published sensitivity analyses are false: A systematic review of sensitivity analysis practices *Environ. Modelling Softw.* **114** 29–39
[31] Sobol I 2001 Global sensitivity indices for nonlinear mathematical models and their monte carlo estimates *Math. Comput. Simul* **55** 271–80 The Second IMACS Seminar on Monte Carlo Methods